

A hybrid self-adaptive Firefly-Nelder-Mead algorithm for structural damage detection

Chu-Dong Pan¹, Ling Yu^{*1,2}, Ze-Peng Chen¹, Wen-Feng Luo¹ and Huan-Lin Liu¹

¹Department of Mechanics and Civil Engineering, Jinan University, Guangzhou 510632, China

²MOE Key Lab of Disaster Forecast and Control in Engineering, Jinan University, Guangzhou 510632, China

(Received November 29, 2015, Revised April 19, 2016, Accepted April 23, 2016)

Abstract. Structural damage detection (SDD) is a challenging task in the field of structural health monitoring (SHM). As an exploring attempt to the SDD problem, a hybrid self-adaptive Firefly-Nelder-Mead (SA-FNM) algorithm is proposed for the SDD problem in this study. First of all, the basic principle of firefly algorithm (FA) is introduced. The Nelder-Mead (NM) algorithm is incorporated into FA for improving the local searching ability. A new strategy for exchanging the information in the firefly group is introduced into the SA-FNM for reducing the computation cost. A random walk strategy for the best firefly and a self-adaptive control strategy of three key parameters, such as light absorption, randomization parameter and critical distance, are proposed for preferably balancing the exploitation and exploration ability of the SA-FNM. The computing performance of the SA-FNM is evaluated and compared with the basic FA by three benchmark functions. Secondly, the SDD problem is mathematically converted into a constrained optimization problem, which is then hopefully solved by the SA-FNM algorithm. A multi-step method is proposed for finding the minimum fitness with a big probability. In order to assess the accuracy and the feasibility of the proposed method, a two-storey rigid frame structure without considering the finite element model (FEM) error and a steel beam with considering the model error are taken examples for numerical simulations. Finally, a series of experimental studies on damage detection of a steel beam with four damage patterns are performed in laboratory. The illustrated results show that the proposed method can accurately identify the structural damage. Some valuable conclusions are made and related issues are discussed as well.

Keywords: structural damage detection (SDD); firefly algorithm; Nelder-Mead algorithm; self-adaptive; finite element model (FEM)

1. Introduction

Structural health monitoring (SHM) technology provides practical platform to evaluate the safety and durability of a structure (Ou and Li 2010, Li *et al.* 2012). It can serve as a tool to develop the methods of life-cycle performance design, evaluation, maintenance and management of a structure (Li *et al.* 2015). Structural damage detection (SDD) is one of the core techniques in the field of SHM and has been widespread concerned by the researchers all over the world (Farrar and Worden 2007). The vibration-based SDD methods are the methods which identify the

*Corresponding author, Professor, E-mail: lyu1997@163.com

damages based on the dynamical characteristic and/or the dynamical responses (Ye *et al.* 2013). Lots of the vibration-based SDD methods have been proposed (Farrar *et al.* 2001, Yan *et al.* 2007) and used for different load conditions, such as earthquake (Li *et al.* 2009), wind (Wang *et al.* 2014) and so on. Generally, the methods can be divided into two groups, i.e. statistics-based SDD methods (Fugate *et al.* 2001, Ye *et al.* 2012, Dorvash *et al.* 2014) and model-based SDD methods. The statistics-based methods are not based on structural models, they are always identify the structural damage only based on the statistical characters of dynamic response signals, such as time series-based method (Gul and Catbas 2011, Yu and Lin 2015), Hilbert-Huang transform method (Chen *et al.* 2014), higher statistical moments method (Yu and Zhu 2015, Yu and Zhu 2016), multi-single techniques (Yi *et al.* 2013), etc. Another group method is usually implemented by finite element analysis; therefore, the identified results are based on the accuracy of structural finite element model (FEM).

The model-based methods can be divided into dynamic fingerprint based methods (Cao *et al.* 2014) and model updating based methods (Yu and Yin 2010). The model updating based methods are often converted into mathematical problem solving constrained multi-objective optimization (Jung *et al.* 2010, Wang *et al.* 2010). The multi-objective optimization problem can be always converted into a single-objective optimization problem with the priori articulation of preferences, such as, weighted sum method, weighted min-max method (Marler and Arora 2004), etc. When the structural responses are free from noise pollution and the FEM is accurate for the real structure, most of objective functions are equivalent. Actually, the noise pollution is inevitable, therefore, how to design a single-objective function or how to evaluate the single-objective function is very important for SDD. The mathematical model of the traditional constrained optimization methods is very complex and cannot be used to solve the high dimensional and complex optimization problems. Fortunately, some swarm intelligence (SI) optimization algorithms are adopted to solve the large-scale civil engineering structural optimization problems (Yu *et al.* 2012), such as PSO algorithm (Shirazi *et al.* 2014, Tang *et al.* 2013), ACO algorithm (Yu and Xu 2011), GAFSA algorithm (Yu and Li 2014), GA algorithm (Yi *et al.* 2011), MA algorithm (Yi *et al.* 2012), WA (Yi *et al.* 2016) algorithm, etc. But there are still some disadvantages, for example, PSO is easy to fall into the local extreme point and it needs too long computation time. While for both ACO and GAFSA, it is hard to determine the key parameters for SDD. The performances of SI algorithms mainly depend on the key parameters (Yang 2014). However, for the structural optimization problems, it is very hard to select the effective key parameters for the SI algorithms.

Inspired by the flashing patterns and behavior of the fireflies, firefly algorithm (FA) is first developed by Yang and widely used (Yang 2010, Fister *et al.* 2013). However, the FA application in the SDD field seems not so much. For FA, there are two important components: exploitation and exploration. Exploration means that the search space is sufficiently investigated on a rough level, while exploitation means that the interesting areas are searched more intensively in order to allow for a good approximation to an optimum (Yang *et al.* 2015). For the classical FA, the exploration component is ensured by the random behavior, while the attraction behavior enhances the exploitation component. However, for any two fireflies, if the distance is very small, the attraction will be very strong, therefore the weaker one will approximately move randomly close to the brighter one. In other word, the weaker firefly will do exploitation behavior with poor efficiency approximately as the pure random search algorithm done. The balance of exploitation and exploration mainly depended on the key parameters of FA. Therefore, the performance of FA is mainly determined by the key parameters tuning and control. The methods for parameter control can be divided into three groups, i.e. fixed control method, random control method and

self-adaptive control. The self-adaptive control method means that the parameter values will vary according to the iterations and/or the characters of the swarm, and it has been widespread concerned by the researchers (Chen and Ding 2015). However, at the moment, there is no efficient method in general for parameter tuning and control.

As an exploring attempt to the SDD problem, a hybrid self-adaptive Firefly-Nelder-Mead (SA-FNM) algorithm is proposed for the SDD problem in this study. The Nelder-Mead (NM) algorithm is incorporated into FA for improving the local searching ability. A new strategy for exchanging the information is used to reduce the computation cost of FA. Both the strategies of random walk and self-adaptive method are introduced to improve the performance of SA-FNM. After that, the SA-FNM is used to solve the SDD problem. Both the numerical simulations and experimental verification are performed.

2. Self-adaptive firefly-nelder-mead algorithm

2.1 Basic firefly algorithm

Firefly algorithm is a new SI optimization algorithm inspired by nature fireflies flashing behavior. In FA, the fireflies abide by the following three rules: 1) all fireflies are unisex so that one firefly will be attracted to other fireflies regardless of their sex; 2) Attractiveness is proportional to their brightness, thus for any two flashing fireflies, the less brighter one will move towards the brighter one. The attractiveness is proportional to the brightness and they both decrease as their distance increases; 3) For a specific problem, the brightness of firefly is associated with the objective function.

The light intensity of a firefly will decrease with the increasing distance of viewer. In addition, light is also absorbed by the media. Therefore, it can be defined as

$$I(r) = I_0 e^{-\gamma r^2} \tag{1}$$

where I_0 is the original light intensity, r is the distance between any two fireflies and γ is the light absorption coefficient. The attractiveness is proportional to the light intensity, which is defined as

$$\beta(r) = \beta_0 e^{-\gamma r^2} \tag{2}$$

where β_0 is the attractiveness at $r = 0$ and always set as $\beta_0 = 1$. The i -th firefly is attracted to the j -th firefly, and the movement is formulated by

$$x_i^d(t+1) = x_i^d(t) + \beta_0 e^{-\gamma r^2} [x_j^d(t) - x_i^d(t)] + \alpha \cdot L_d(\text{rand} - 0.5) \tag{3}$$

where α is the randomization parameter and always be controlled as Eq. (10). L_d is the d -th dimension length of the searching region, rand is a random number generator uniformly distributed in $[0, 1]$. r is the distance between i -th firefly and j -th firefly, which is defined as the Cartesian distance as

$$r = \|\mathbf{x}_i - \mathbf{x}_j\| \tag{4}$$

2.2 Strategy for improving the basic firefly algorithm

2.2.1 Nelder-Mead algorithm

In order to improve the local searching ability, the NM algorithm is introduced into combined with FA. The NM algorithm, introduced by Nelder and Mead in 1965, is a non-derivative searching method for multidimensional unconstrained minimization. According to the NM algorithm, the worst point of n-simplex will be replaced by a better one calculated by four basic conversions, i.e., reflection, expansion, contraction and shrink. In the proposed algorithm, only 2-dimension NM algorithm and three basic conversions (reflection, expansion and contraction as shown in Fig. 1) are used. The basic process is proposed as follows:

a) For any two fireflies, as shown in Fig. 2(a), if the distance satisfies $r < r_{NM}$ and $r \neq 0$, the weaker ones will move as the NM algorithm done, else it will move as the basic FA done. Here r_{NM} is the critical distance between FA and NM.

b) For the NM algorithm, a random point will be created near to the better one, and its possible region is decided as a hyper-sphere. The center point is the better position and the radius is the distance between the two fireflies, as shown in Fig. 2(b).

c) For the NM algorithm, the two fireflies and the random point are taken as the input-data for 2-dimension NM algorithm with three basic conversions, i.e., reflection, expansion and contraction for one generation. If any point (created by reflection, expansion, outside-contraction or inside-contraction) is found better than the best point among the 3 points of a 2-simplex, the weaker one will move to the better one, else the weaker one will move to the random point.

2.2.2 Exchange of information

In the basic FA, one firefly will be attracted by all the better ones, therefore, the time complexity of FA is $O(N^2)$, where N is the number of fireflies. As a matter of fact, the attraction between any two fireflies is very small when the distance is large. In order to reduce the computation cost of SA-FNM, a new strategy of exchange information is proposed as follows:

a) Each firefly is attracted by only one in a group.

b) For any one firefly, if the distance to the best firefly is small than r_{NM} and not equal to zero, it will be attracted by the best firefly with NM algorithm, else it will be attracted by the one with best attractiveness $\beta(r)$. The time complexity of improved SAFA-NM is $O(N)$.

2.2.3 Random walk

A random walk strategy is introduced to improve the behavior of the best firefly. The best firefly will be regard as a random walker. The random walker will move randomly step by step in the feasible region to find the better fitness value. The best firefly will be replaced by a position with a better fitness value. The process can be defined as

$$\begin{aligned} x^d(t+1) &= x^d(t) + \alpha_r \times L_d \times rand, \\ t &= 1, 2, 3, \dots, N_r \end{aligned} \quad (5)$$

where $x^d(t)$ is the d -th dimension of the position at t -th step. t, N_r are the t -th step and the maximum steps, respectively. α_r is the step length. L_d is the d -th dimension length of the searching region. $rand$ is a random generator uniformly distributed in $[-1, 1]$.

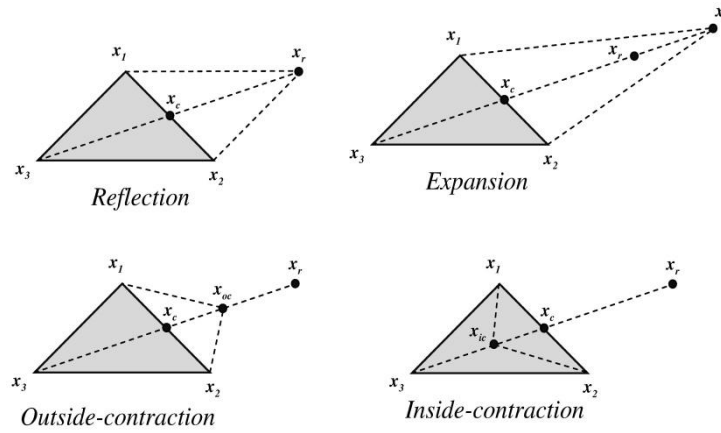
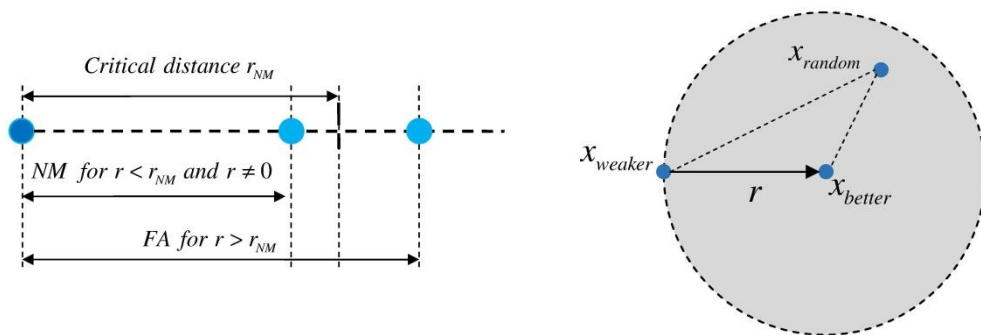


Fig. 1 Basic conversions of NM algorithm



(a) Criterion for firefly movement

(b) Possible region of random point

Fig. 2 Criterion for firefly movement and possible region of random point in SA-FNM

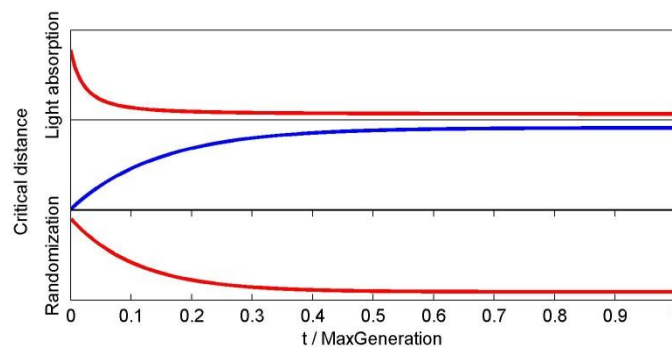


Fig. 3 Generation trends of three key parameters for a constant maximum group radius

2.2.4 Self-adaptive strategy

The light intensity is absorbed by the surrounding and the information will decrease with the increasing distance. Therefore, the distances among the fireflies play an important role in the SA-FNM. In the group based SI algorithm, the group radius is always used to describe the distance feature of the swarm. The group radius is defined as

$$R = \frac{1}{N} \left(\sum_{i=1}^N \| \mathbf{x}_i - \mathbf{x}_c \|_2 \right) \quad (6)$$

where N is the number of fireflies; \mathbf{x}_i is the position of i -th firefly; \mathbf{x}_c is the swarm group center and always defined as

$$\mathbf{x}_c = \frac{1}{N} \left(\sum_{i=1}^N \mathbf{x}_i \right) \quad (7)$$

There are three key parameters to be tuned for better performance of SA-FNM. They are light absorption γ , critical distance r_{NM} and randomization parameter α , respectively. Generally, the SA-FNM will do a global searching with the large γ , small r_{NM} and large α , otherwise the SA-FNM will do a local searching with small γ , large r_{NM} and small α . The algorithm is usually good at global searching during the front generations, while it has a good ability at local searching during the last generations. The three key parameters can be turned and controlled according to the maximum group radius as

$$\gamma(t) = -\frac{\ln(0.01)}{(2v_y R_{max})^2}, \quad v_y = 0.1 + \left[1 - \left(\frac{0.1}{1} \right)^{\frac{t}{G}} \right] \quad (8)$$

$$r_{NM}(t) = 2v_r R_{max}, \quad v_r = 10^{-4} + 0.1 \left[1 - \left(\frac{10^{-4}}{0.1} \right)^{\frac{t}{G}} \right] \quad (9)$$

$$\alpha(t) = 0.9 \left(\frac{10^{-4}}{0.9} \right)^{\frac{t}{G}} \quad (10)$$

where t , G are the t -th generation and maximum generations, respectively. R_{max} is the maximum group radius during the first $t-1$ generations. The self-adaptive strategy of $\alpha(t)$ is widely used in the basic FA. The generation trends of three key parameters are shown in Fig. 3. It clearly shows that both the light absorption and randomization parameter are reduced during the generation, while the critical distance has an opposite trend. The flowchart of SA-FNM can be summarized as shown in Fig. 4.

2.3 Benchmark function study

In order to evaluate the performance of SA-FNM, a suite of three famous benchmark functions

are employed as shown in Table 1. All the global minimum values are equal to zero. The benchmark function Sphere is single-peak function, while other benchmark functions are multi-peak function, which have multiple local minimum values. Both the basic FA and the SA-FNM are used to solve the problems. The maximum generation $G=200$ and the population size $N=25$. The number of random walk $N_r=20$ and the step length $\alpha_r=0.1$. 50-time runs are calculated for each case.

It can be found from Table 2 that the SA-FNM can find the minimum value for all the benchmark functions. Compared to the basic FA, the SA-FNM can find a much better result with less computation cost. Therefore, the SA-FNM can be hopefully applied to the continuous optimization on SDD in the following section.

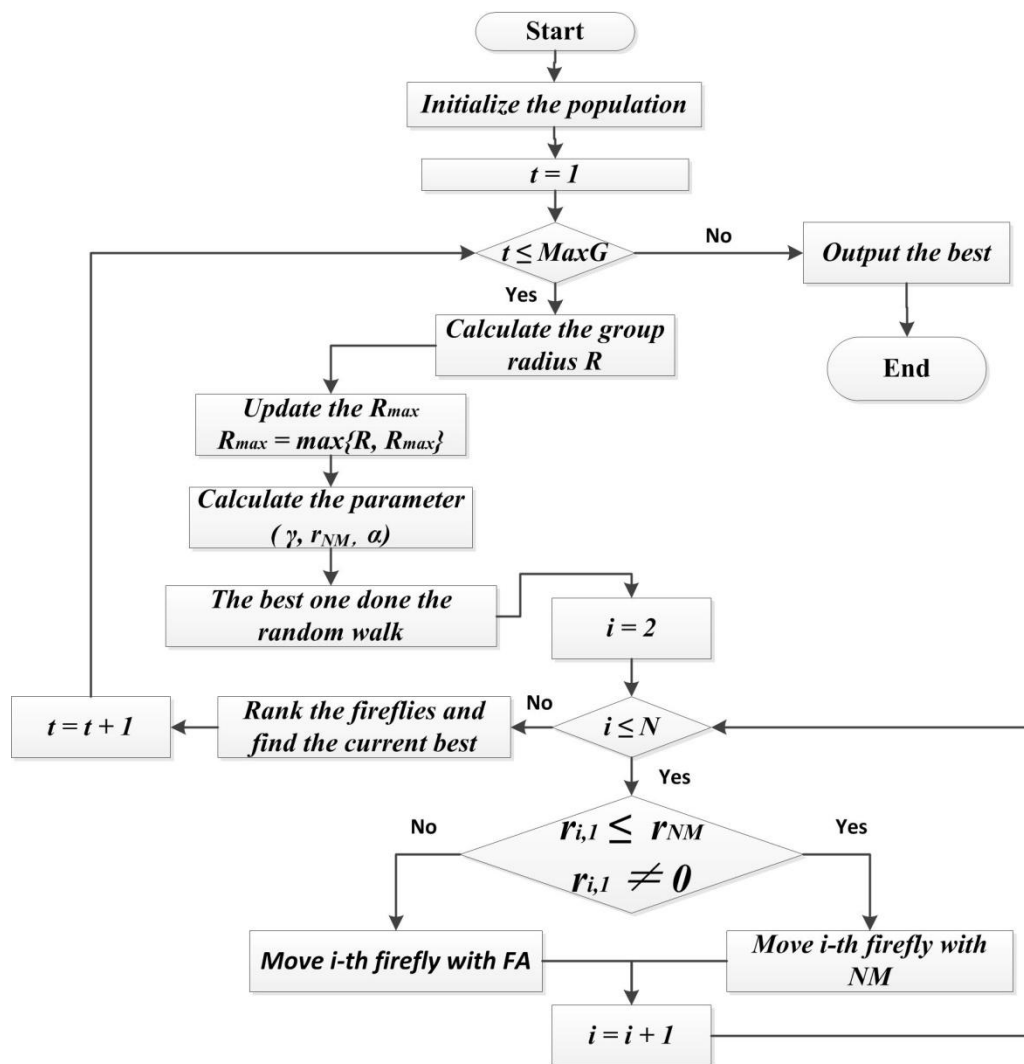


Fig. 4 Flowchart of SA-FNM

Table 1 Three benchmark functions

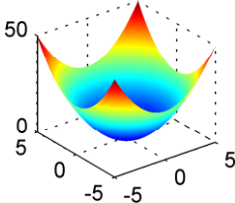
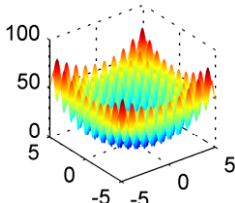
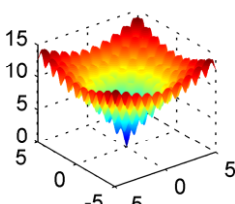
Function	Function expression	Argument range	Global minimum	Landscape
Sphere	$f_1(x, y) = x^2 + y^2$	$[-5, 5]$	$f_1(x, y) = 0$	
Rastrigin	$f_2(x, y) = x^2 + y^2 - 10\cos(2\pi x) - 10\cos(2\pi y) + 20$	$[-5, 5]$	$f_2(x, y) = 0$	
Ackley	$f_3(x, y) = 20 - 20e^{(-0.2\sqrt{0.5(x^2+y^2)})} - e^{(0.5[\cos(2\pi x) + \cos(2\pi y)])} + e$	$[-5, 5]$	$f_3(x, y) = 0$	

Table 2 Performance comparisons on FA and SA-FNM

Function	Calculated performance	FA	SA-FNM
Sphere	Best fitness value	5.352×10^{-12}	6.803×10^{-142}
	Average fitness value	2.199×10^{-10}	7.136×10^{-132}
	Average CPU time	1.087 s	0.426 s
Rastrigin	Best fitness value	3.866×10^{-10}	0.000×10^0
	Average fitness value	5.970×10^{-2}	1.990×10^{-2}
	Average CPU time	0.883 s	0.366 s
Ackley	Best fitness value	2.905×10^{-6}	0.000×10^0
	Average fitness value	3.206×10^{-5}	0.000×10^0
	Average CPU time	1.912 s	0.543 s

3. Description of SDD problem

3.1 SDD Mathematic model

Generally, for a SDD problem, only the stiffness is considered to reduce while ignoring the change of the mass, as

$$\mathbf{K} = \mathbf{K}_0 - \sum_i^N \alpha_i \mathbf{K}_i \tag{11}$$

where \mathbf{K}, \mathbf{K}_0 is the global stiffness matrix of the damaged and undamaged structure, respectively. α_i is the coefficient of i -th element stiffness damage, \mathbf{K}_i is the expanded stiffness matrix of the i -th element in the global coordinate system. The motion equation of the damaged structure can be expressed as follows

$$\mathbf{K}\boldsymbol{\varphi}_j = \lambda_j \mathbf{M}_0 \boldsymbol{\varphi}_j \tag{12}$$

where \mathbf{M}_0 is the mass matrix of structure, $\boldsymbol{\varphi}_j$ is the j -th mode shape of structure, $\lambda_j = (2\pi f_j)^2$ and f_j is the j -th frequency of structure. Therefore, $(\lambda_j^\alpha, \boldsymbol{\varphi}_j^\alpha)$ can be obtained by solving Eqs. (11)-(12) with the damage coefficient vector of element stiffness $\boldsymbol{\alpha} = [\alpha_1, \alpha_2, \alpha_3, \dots, \alpha_N]$.

Similar to the model updating methods, the objective functions used in most of the former research of SDD problem are try to minimize the difference between the test values and the calculated values from FEM without using the healthy information. Actually, the model updating problem is try to minimize the model error, therefore, the initial model error do not play an important role in the results. However the SDD problem is focus on the change of the real structure and the accuracy of the calculated FEM will affect the identified results. Therefore, it is better to consider the healthy information in the objective function because some of the model errors are contained in the healthy information. Then the SDD problem can be transformed into the following constrained optimization problem:

$$\begin{aligned} \min f(\boldsymbol{\alpha}) &= \sum_{i=1}^s \left[DF(\boldsymbol{\varphi}_i^\alpha - \boldsymbol{\varphi}_i^{ah}, \boldsymbol{\varphi}_i^t - \boldsymbol{\varphi}_i^{th}) + ER(f_i^\alpha - f_i^{ah}, f_i^t - f_i^{th}) \right] \\ \text{subject to: } &0 \leq \alpha_j < 1, j = 1, 2, 3, \dots, N \end{aligned} \tag{13}$$

where s is the number of measured modes. f_i^{th} and $\boldsymbol{\varphi}_i^{th}$ are the i -th nature frequency and mode shape of the real healthy structure, respectively. f_i^t and $\boldsymbol{\varphi}_i^t$ are the i -th nature frequency and mode shape of the test structure. f_i^{ah} and $\boldsymbol{\varphi}_i^{ah}$ are the i -th nature frequency and mode shape of the FEM healthy state. f_i^α and $\boldsymbol{\varphi}_i^\alpha$ are the i -th nature frequency and mode shape of the FEM with damage vector $\boldsymbol{\alpha}$. All the mode shapes should be normalized by the same method. The function of $DF(\boldsymbol{\varphi}_i^\alpha - \boldsymbol{\varphi}_i^{ah}, \boldsymbol{\varphi}_i^t - \boldsymbol{\varphi}_i^{th})$ and $ER(f_i^\alpha - f_i^{ah}, f_i^t - f_i^{th})$ are defined as follows:

$$DF(\varphi_i^a - \varphi_i^{ah}, \varphi_i^t - \varphi_i^{th}) = \left(\frac{\|(\varphi_i^a - \varphi_i^{ah}) - (\varphi_i^t - \varphi_i^{th})\|_2}{\|\varphi_i^{th}\|_2} \right)^2 \tag{14}$$

$$ER(f_i^a - f_i^{ah}, f_i^t - f_i^{th}) = \left(\frac{|(f_i^a - f_i^{ah}) - (f_i^t - f_i^{th})|}{f_i^{th}} \right)^2 \tag{15}$$

3.2 Multi-step method

In order to identify the structural damage more exactly, the multi-step method will be studied in this paper. The multi-step was proposed by Shirazi (2014). In the study, the information of healthy elements will be found in the previous step. A self-adaptive scheme is also used to avoid identifying a damaged element as a healthy one. However, the faulty judgment may be occurred especially for the small damage. Actually, the essence of multi-step is a reducing dimension method with preferences. The purpose of multi-step is to find a better point according to the objective function. Therefore, the final result should be taken as the one with best fitness value among all the step results, but not the last step result. More information of the proposed multi-step method is illustrated as below.

First of all, the SA-FNM will be used to solve the SDD problem. Then the undamaged elements will be picked out by the threshold value ζ . This process can be expressed as

$$element_i = \begin{cases} damage, & \alpha_i \geq \zeta \\ undamage, & \alpha_i < \zeta \end{cases} \tag{16}$$

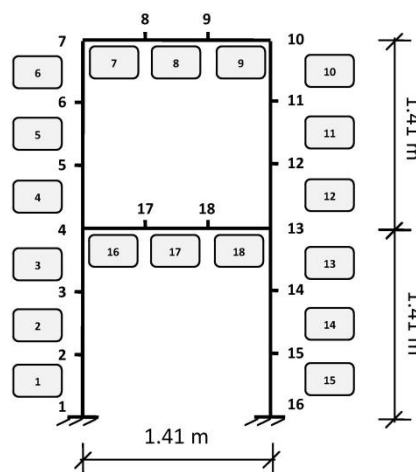


Fig. 5 Finite element model of two-storey rigid frame

Then the undamaged elements will be setting as known conditions for the next step. It means that the Eq. (13) can be rewritten as

$$\begin{aligned} \min f(\alpha) &= \sum_{i=1}^s [DF(\varphi_i^a - \varphi_i^{ah}, \varphi_i^t - \varphi_i^{th}) + ER(f_i^a - f_i^{ah}, f_i^t - f_i^{th})] \\ \text{subject to: } &\begin{cases} 0 \leq \alpha_j < 1, & j \in \text{damaged elements} \\ \alpha_j = 0, & j \in \text{undamaged elements} \end{cases} \end{aligned} \tag{17}$$

The above problem can be solved by SA-FNM and this process can be redone as a next step. The result of the best fitness value among all the step results will be taken as the final result.

4. Numerical Simulations on SDD

4.1 SDD on two-storey rigid frame

The FEM of two-storey rigid frame is shown in Fig. 5. Both the height and width at each storey are 1.41 m and the structure is divided into 18 elements. The structure is simulated with the following parameters as shown in Table 3.

The parameters of SA-FNM are set as follows: maximum generation $G=200$ and swarm population $N=40$. Number of random walk $N_r=20$ and step length $\alpha_r=0.1$. The threshold value $\zeta = \max(\alpha_i) \times 5\%$ and α_i is the results of the front step. Two-steps are used to improve the identified results. The identified result is taken as the best fitness value of 5-time running results.

Some asymmetric damage and symmetric damage cases are studied, respectively, as shown in Table 4. The first five modes are used to build the objective function. Only the horizontal freedoms of the column and the vertical freedoms of the beam are picked out for calculating. Two noise levels 0% and 1% are added to the mode shapes to study the anti-noise performance of proposed method. The frequency and mode shapes with noise pollution can be calculated as

$$f_n = f(1 + N_L \times \mathbf{Rand}) \tag{18}$$

$$\varphi_n = \varphi(1 + N_L \times \mathbf{Rand}) \tag{19}$$

where f_n , φ_n are the frequency and mode shape with noise pollution, respectively. f , φ are the frequency and mode shape without noise pollution, respectively. N_L is the noise level. \mathbf{Rand} is a random generators uniformly distributed in $[-1, 1]$.

Table 3 Simulation parameters of two-storey rigid frame

	Elastic modulus	Moment of inertia	Cross-sectional area	Density
Column	$2 \times 10^{11} \text{ N} \bullet \text{m}^{-2}$	$1.26 \times 10^{-5} \text{ m}^4$	$2.98 \times 10^{-3} \text{ m}^2$	$8590 \text{ kg} \bullet \text{m}^{-3}$
Beam	$2 \times 10^{11} \text{ N} \bullet \text{m}^{-2}$	$2.36 \times 10^{-5} \text{ m}^4$	$3.2 \times 10^{-3} \text{ m}^2$	$7593 \text{ kg} \bullet \text{m}^{-3}$

Table 4 Four cases for simulation of two-storey rigid frame

Case	Type	Damage extents @ element
1		5% @8
2	asymmetric	15% @8, 15% @17
3		10% @8, 20% @11, 15% @17
4	symmetric	10% @5, 10% @11

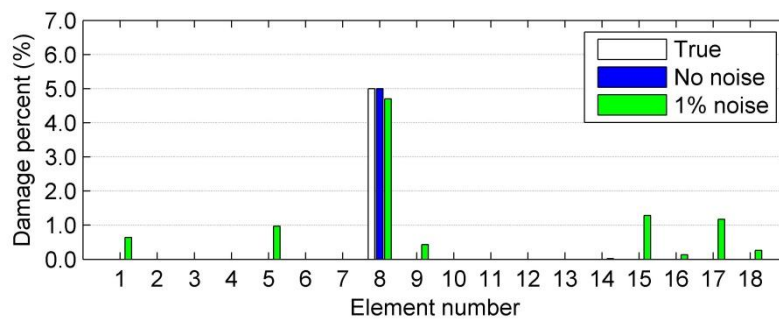


Fig. 6 SDD results for element 8 damaged by 5%

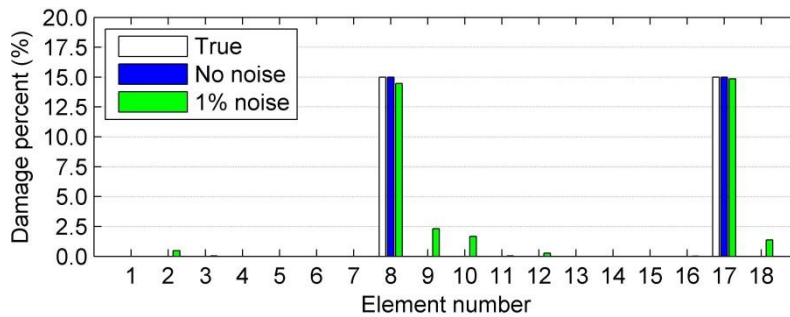


Fig. 7 SDD results for elements 8 and 17 damaged by 15% and 15%, respectively

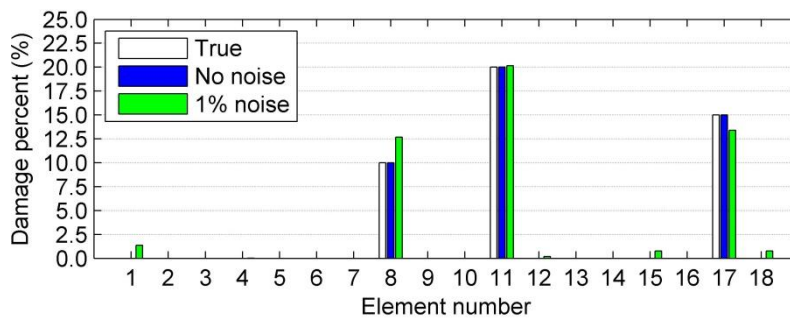


Fig. 8 SDD results for elements 8, 11 and 17 damaged by 10%, 20% and 15%, respectively

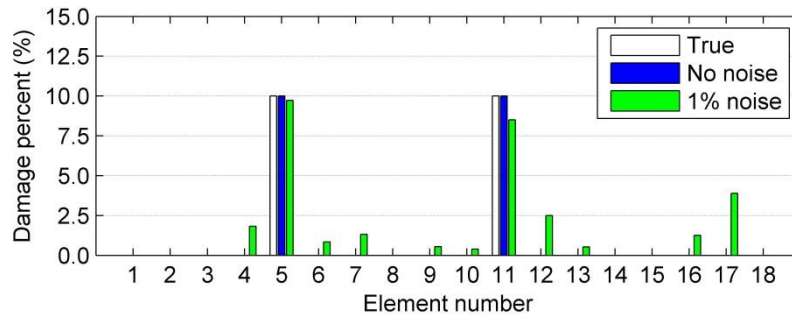


Fig. 9 SDD results for elements 5 and 11 damaged by 10% and 10%, respectively

The SDD results of asymmetric damage cases are shown in Figs. 6-8 and the symmetric cases are shown in Fig. 9. As shown in Fig. 6, it can be seen that the SA-FNM can identify the single damage location and weak damage extent with better noise immunity. The damage location and extent can be accurately identified for no noise cases. It means that the SA-FNM can find the global optimal value of the objective function. Small misjudgment will be occurred at some elements if the noise pollution is considered. The damage extents at the misjudgment elements are quiet smaller than the identified damage extents at the real damage elements. The main reason for the issues is that the mode shapes are not sensitive to the minimal changes of the structure, therefore, the mode shapes component in objective function is sensitive to the noise and the extreme point of the objective function easily changes if the noise pollution is considered. From Figs. 7 and 8, the same conclusions can be made for the two and multi-damage condition. It can be seen from Fig. 9 that the SA-FNM can identify both the damage location and damage extents for symmetric damage cases, while the misjudgment ratio is larger than asymmetric damage conditions if the noise pollution is considered.

4.2 SDD on a steel beam

A steel beam with 3 meter long is shown in Fig. 10. The beam was uniformly divided into 20 elements. The line density $\rho A = 9.07920 \text{ kg} \cdot \text{m}^{-1}$ and the flexural rigidity $EI = 1.53092 \times 10^5 \text{ N} \cdot \text{m}^2$. The coefficients of vertical spring are $k_0 = k_1 = 1.5 \times 10^7 \text{ N} \cdot \text{m}^{-1}$, respectively. The spring coefficients of torsional spring are $k_{01} = k_{11} = 1.5 \times 10^4 \text{ N} \cdot \text{rad}^{-1}$, respectively.

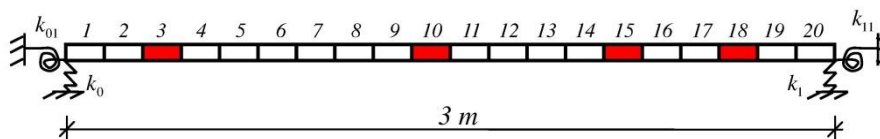


Fig. 10 Finite element model of steel beam

Table 5 First five frequencies of steel beam

Model	Frequencies				
	1 st mode	2 nd mode	3 rd mode	4 th mode	5 th mode
Real steel beam f^r / Hz	23.7439	89.1031	190.7966	316.6420	452.9506
Calculated FEM f^c / Hz	23.7601	89.0725	190.5597	315.8576	451.3579
Error $(f^c - f^r) / f^r \times 100\%$	0.07%	-0.03%	-0.12%	-0.25%	-0.35%

Table 6 Four cases for steel beam SDD simulations

Cases	Type	Damage extents @ element	Noise level	
			Frequency	Mode shape
1	Single damage	15% @3	0%	0%
			0.5%	0.5%
2	Two damage & asymmetric	15% @3, 20% @15	0%	0%
			0.5%	0.5%
3	Two damage & symmetric	20% @3, 20% @18	0%	0%
			0.5%	0.5%
4	Multi-damage	20% @3, 25% @10, 15% @15	0%	0%
			0.5%	0.5%

The model error was considered in this section. For the calculated FEM, the coefficient of left vertical spring $k_0 = 1.45 \times 10^7 \text{ N} \cdot \text{m}^{-1}$ and the coefficient of right torsional spring $k_{11} = 1.55 \times 10^4 \text{ N} \cdot \text{rad}^{-1}$. Comparisons on first five frequencies of steel beam are shown in Table 5. Four damage cases are set as shown in Table 6. In order to study the anti-noise performance of proposed method, small noise level is added into frequency and shape mode as well. The first five modes are used to build the objective function. Only the vertical freedoms of the beam are picked out for calculating. The parameters of SA-FNM are set as the same in section 4.1.

The SDD results without and with model error are shown in Table 7. It can be seen that the SA-FNM can accurately identify the damage location and damage extent for four damage cases without model error. That means the SA-FNM can effectively find the global optimal value of the objective function. From the SDD results with model error, it can be seen that most of the elements detection results are not influenced by the model error at supports. Most of the damage extents at damaged elements are slightly small than the true ones. Therefore, the proposed SA-FNM method is not sensitive to the model error at supports.

Table 7 Comparison on damage detection results

True damage		Identified damage	
Extents @ element	With model error?	Correct location	Wrong location (if extent>1%)
15% @3	No	15% @3	-
	Yes	14.8% @3	-
15% @3, 20% @15	No	15% @3, 20% @15	-
	Yes	14.8% @3, 20% @15	-
20% @3, 20% @18	No	20% @3, 20% @18	-
	Yes	19.7% @3, 19.9% @18	1.1% @2
20% @3, 25% @10, 15% @15	No	20% @3, 25% @10, 15% @15	-
	Yes	19.8% @3, 25% @10, 14.8% @15	1.9% @1

The SDD results with model error and noise pollution are shown in Figs. 11-14. From Fig. 11, it can be seen that the identified accuracy is reduced when the noise pollution is considered at true damage element. Misjudgments occur at some elements sometimes. The main reason for the phenomenon is that the first five modes data are not sensitive to a minimal change in the steel beam. Therefore, the extreme point of the objective function is easily shifted under noise pollution. From Figs. 12-14, the same conclusions can be made for two and multi-damage cases. Taken all the SDD results considered together, it can be seen that large misjudgments always occur at element 1 and element 20, which indicates that the SDD results on elements near to the supports are more sensitive to the noise.

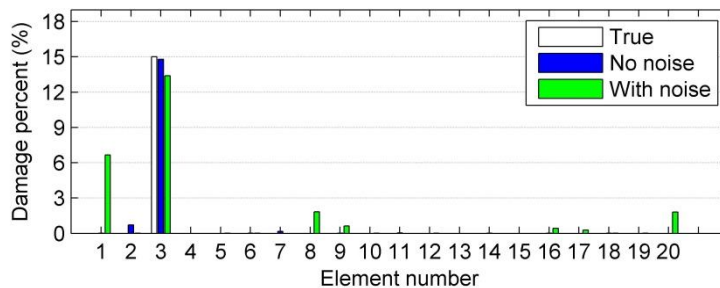


Fig. 11 SDD results for element 3 damaged by 15%

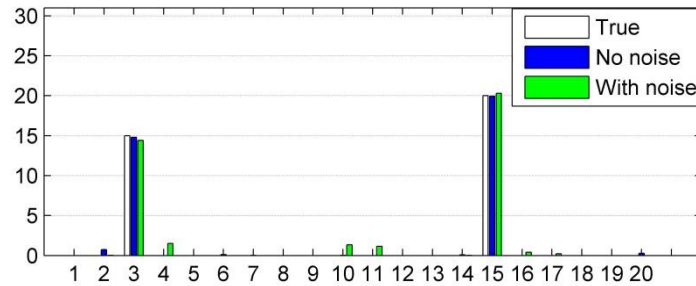


Fig. 12 SDD results for element 3 and element 15 damage by 15% and 20%, respectively

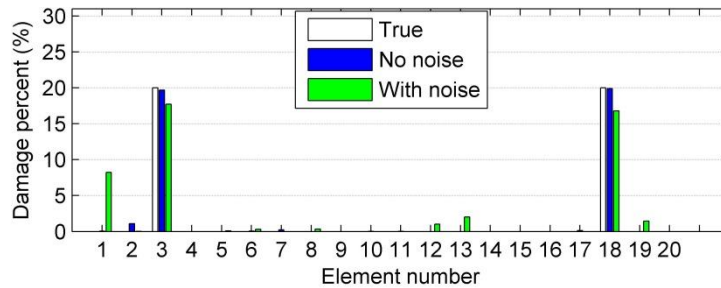


Fig. 13 SDD results for elements 3 and 18 damaged by 20% and 20%, respectively

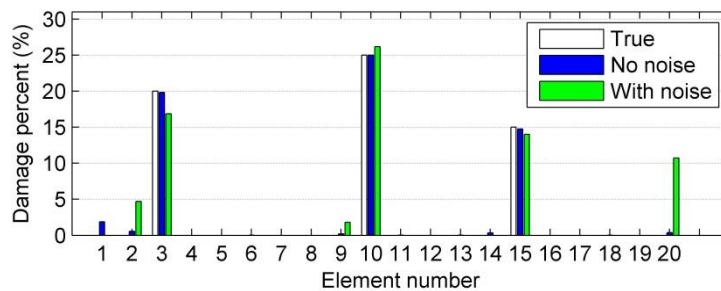


Fig. 14 SDD results for elements 3, 10 and 15 damaged by 20%, 25% and 15%, respectively

5. Experimental validations

5.1 Experimental setup

To verify the proposed method in laboratory, a series of experiments on a hinge supported beam were carried out, as shown in Fig. 15. The span of the test steel beam is 3 m. The cross section is a rectangular tube with 140 mm width and 60 mm height. The wall thickness is 3 mm.

As shown in Fig. 16, a vibrator (HEV-200) together with a power amplifier and a force sensor

(PCB, 208C02) were mounted on the beam at 1.65 m from the left support. A periodic Chirp excitation vertically with a bandwidth from 0 Hz to 512 Hz is generated by LMS Test.Lab. The acceleration sensors (PCB, ICP 333B30) were mounted on the middle line of lower surface. Each complete model test contains two step runs. Eleven sensors were mounted on points 1, 3, 5, 7, 9, 11, 13, 15, 17, 19, 21 for the first run. They were mounted on points 2, 4, 5, 6, 8, 10, 12, 14, 16, 18, 20 for second run. The point 5 is used as a reference point for merging the two runs. The sampling frequency was 2048 Hz and the sampling duration is 1s for each data block. In order to reduce the effect of noise, the frequency response function was taken as the average of 100 times run and the average type is linear amplitude average. All the responses were collected by LMS Test.Lab and stored into the personal computer.



Fig. 15 Experimental setup

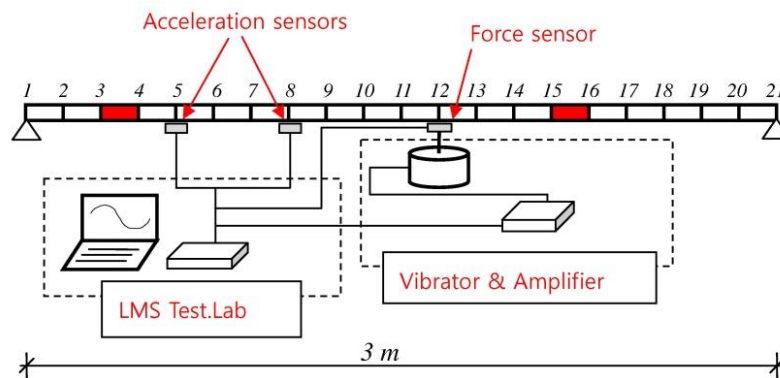


Fig. 16 Simple diagram of experiment

5.2 Model updating

The initial FEM of the steel beam can be set up as the steel beam in section 4.2, as shown in Fig. 10. Six parameters are selected to be updated. They are steel density, elastic modulus, two vertical spring coefficients and two torsional spring coefficients. The objective function for model updating is defined as

$$\min f(\mathbf{p}) = \sum_{i=1}^3 [DF(\varphi_i^p, \varphi_i^t) + ER(f_i^p, f_i^t)] \tag{20}$$

where f_i^t and φ_i^t are the i -th test nature frequency and mode shape, respectively. f_i^p and φ_i^p are the i -th calculated nature frequency and mode shape, respectively. \mathbf{p} is the parameters vector for updating. The parameters of SA-FNM are the same as in section 4.1. The constraint conditions for all the updating values are shown in Table 8. The comparisons on the first three frequencies from both experimental and updated FEM are shown in Table 9. The first three mode shapes of measured and the updated FEM are shown in Fig. 17. From Table 9 and Fig. 17, it clearly shows that the SA-FNM method can effectively solve the model updating problem of the steel beam.

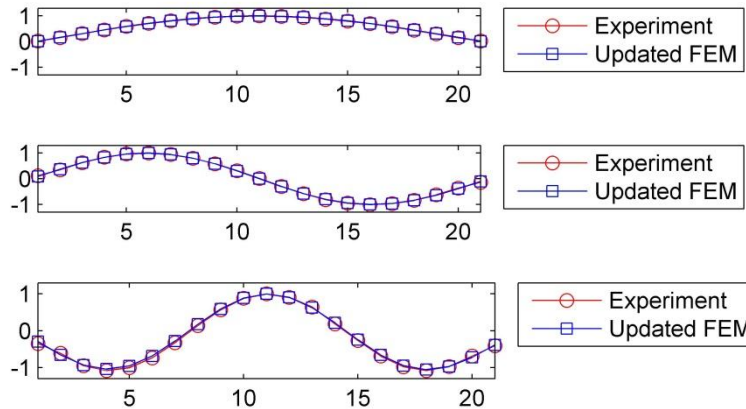


Fig. 17 Comparisons on first three mode shapes of steel beam

Table 8 Constraint conditions for updating values

Updating value	Constraint	Updating value	Constraint
Density kg/m^3	[6500, 8500]	Vertical spring coefficient N/m	[1e6, 1e8]
Elastic modulus Pa	[1.5e11, 2.5e11]	Torsion spring coefficients N/rad	[1e2, 1e5]

Table 9 Comparison on first three frequencies of steel beam

	Frequencies		
	1 st order	2 nd order	3 rd order
Test f^t / Hz	23.650	88.667	188.572
Updated FEM f^p / Hz	23.788	88.232	188.375
Error $(f^p - f^t) / f^t \times 100\%$	0.58%	-0.49%	-0.10%

5.3 SDD of steel beam

The updated FEM can be employed as the benchmark of health structure to simulate the damage cases. The structural damage can be made by reducing the cross-section of the beam as shown in Fig. 18. The true damage extent is estimated by the reduced percentage of beam stiffness. The reduced stiffness can be approximately calculated by change in the inertia moment as follow

$$\alpha_r = 1 - \frac{I_d}{I_h} \tag{21}$$

where α_r is the true damage extent. I_h , I_d are the inertia moment of healthy and damaged cross-section, respectively. As shown in Fig. 19, the inertia moment of healthy and damaged cross-section can be calculated as follows

$$I_h = \frac{BH^3 - bh^3}{12} \tag{22}$$

$$I_d = \frac{Be_1^3 - bf^3 + 2te_2^3}{3} \tag{23}$$

where

$$e_1 = \frac{2td^2 + bt^2}{2(2td + bt)} \tag{24}$$

Four damage patterns are considered in the laboratory, as shown in Table 10. The cutting positions were selected at 0.4 m and 2.2 m from the left end support. The true damage extents were calculated by Eqs. (21)-(24). The measured nature frequencies under four damage patterns were shown in Table 10. It shows that the first three frequencies decrease with increasing damage extent. All the SDD parameters for the proposed algorithm are taken as the same in section 4.1.

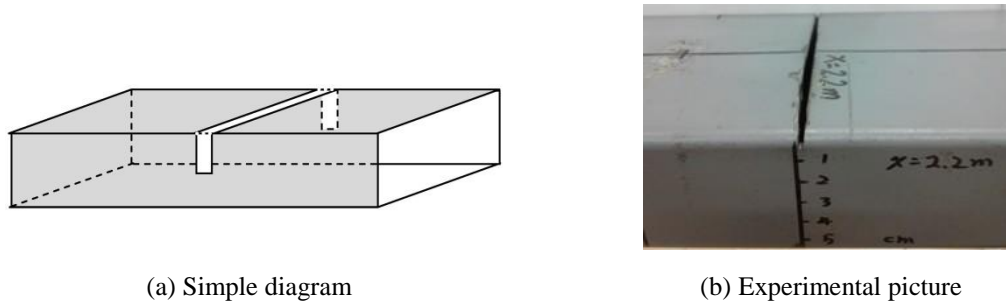


Fig. 18 Cutting mode for making damage

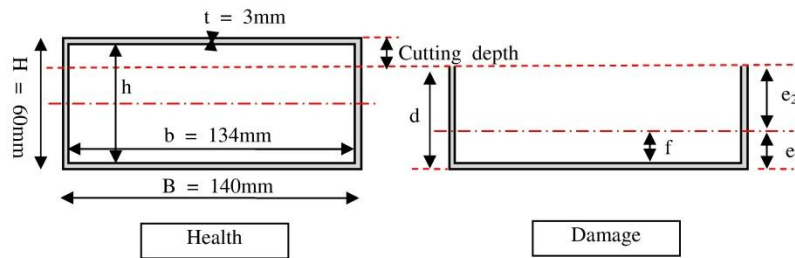


Fig. 19 Cross-section used to approximately estimate true damage extent

Table 10 Four damage patterns for experimental study

Patterns	Cutting depth @ position	Damage extent @ Element	Measured frequencies/Hz		
			1 st order	2 nd order	3 rd order
1	3mm@0.4m	70.1% @3	23.506	86.869	181.350
2	30 mm@0.4m	95.2% @3	22.654	78.822	165.046
3	30mm@0.4m, 3mm@ 2.2m	95.2% @3, 70.1@15	22.241	74.902	161.505
4	30mm@0.4m, 30mm@2.2m	95.2% @3, 95.2@15	19.918	66.492	155.469

The SDD results are shown in Figs. 20-23. As shown in Fig. 20, it can be seen that the SA-FNM method can accurately identify the single damage location and damage extent. The identified damage extent at element 3 is smaller than the true damage extent. Because the true damage extent calculation method used here is an approximate estimation method. Some misjudgments are identified at the healthy elements. The damage extents at the misjudgment elements are quiet smaller than the identified damage extent at element 3. The main reason for the issues is that there are noises in the measured data. From Figs. 21-23, the some conclusions can be made for single and two damage patterns. Also it can be seen that all the identified damage extents of element 4 are bigger than 40%. It seems that the cutting gap for three cases of 30 mm depth at 0.4 m not only affects element 3 but also element 4, which is more consistent with the real damage situations. Therefore, the introduction of the SA-FNM into the SDD problem is feasible and effective.

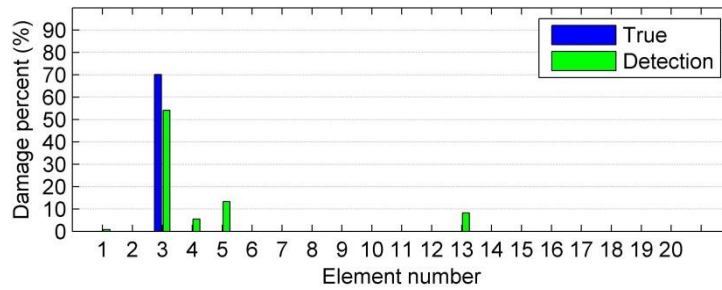


Fig. 20 SDD results for cutting 3mm@0.4m

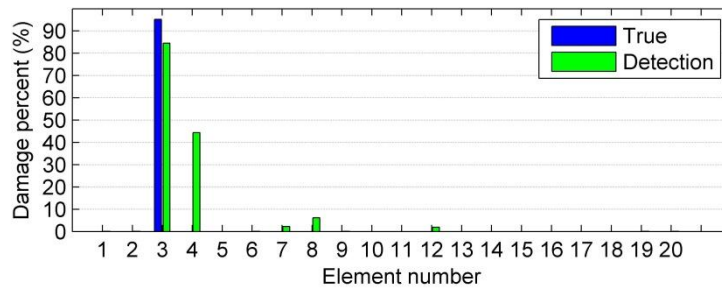


Fig. 21 SDD results for cutting 30mm@0.4m

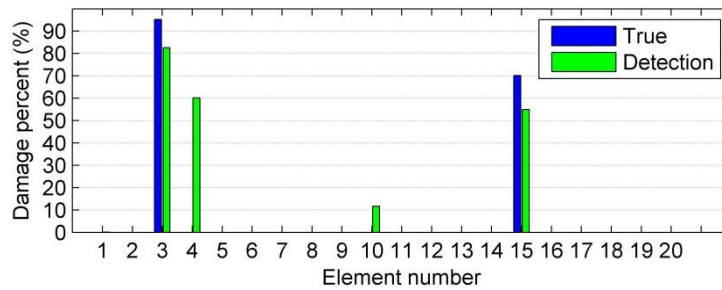


Fig. 22 SDD results for cutting 30mm@0.4m and 3mm@2.2m, respectively

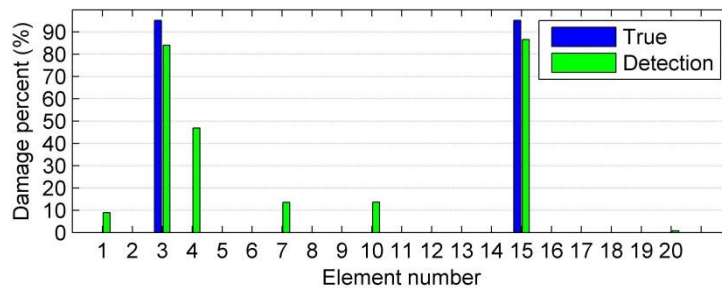


Fig. 23 SDD results for cutting 30mm@0.4m and 30mm@2.2m, respectively

6. Conclusions

A hybrid self-adaptive Firefly-Nelder-Mead (SA-FNM) algorithm is proposed for structural damage detection (SDD) in this study. The basic principle of firefly algorithm (FA) is introduced. The Nelder-Mead (NM) algorithm is incorporated to improve the local searching ability of FA. Some new strategies on information exchange, random walk and self-adaptive method are then used to improve the performance of SA-FNM for solving the SDD problem. Combined with the properties of SDD problem, the multi-step method is proposed. A two-storey rigid frame structure without model error and a steel beam with model error are taken as examples for numerical simulations. Finally, a series of experimental studies on damage detection of a steel beam are performed in laboratory for further verifying the practicability of the proposed SA-FNM method. The following conclusions can be made.

1) The performance of both the basic FA and the proposed SA-FNM are assessed using three test functions. The results show that both the computational accuracy and computation cost due to the proposed SA-FNM are better than ones by the basic FA.

2) A two-storey rigid frame is adopted to do numerical simulations for single, two and multiple damages of structure. The results show that the proposed SA-FNM method can effectively identify damage location and damage extent. Tiny misjudgment will be occurred if the noise pollution is considered.

3) A steel beam with model error is also taken as example for numerical simulation study. The results show that the small model error at supports will mildly affect the SDD results. The identified accuracy will be reduced with considering the noise pollution. The elements near to the end supports are more sensitive to the measured noise.

4) To verify the proposed method in laboratory, a series of experiments on a hinge supported beam are carried out. It can be found that the first three frequencies will decrease with increasing damage extent. The results of model updating show that the SA-FNM can effectively solve a model updating problem of steel beam. The illustrated SDD results show that the SA-FNM can effectively identify both damage location and damage extent with a better noise immunity. Therefore, the introduction of the SA-FNM into the SDD problem is feasible and effective.

Acknowledgments

The project is jointly supported by the National Natural Science Foundation of China with Grant Numbers 51278226 and 50978123.

References

- Cao, M., Radziński, M., Xu, W. and Ostachowicz, W. (2014), "Identification of multiple damage in beams based on robust curvature mode shapes", *Mech. Syst. Signal Pr.*, **46**(2), 468-480.
- Chen, B., Zhao, S.L. and Li, P.Y. (2014), "Application of Hilbert-Huang transform in structural health monitoring: a state-of-the-art review", *Math. Probl. Eng.*, 2014.
- Chen, G. and Ding, X. (2015), "Optimal economic dispatch with valve loading effect using self-adaptive firefly algorithm", *Appl. Intell.*, **42**(2), 276-288.
- Dorvash, S., Pakzad, S.N. and LaCrosse, E.L. (2014), "Statistics based localized damage detection using vibration response", *Smart Struct. Syst.*, **14**(2), 85-104.

- Farrar, C.R. and Worden, K. (2007), "An introduction to structural health monitoring", *Philos. T. R. Soc. A.*, **365**(1851), 303-315.
- Farrar, C.R., Doebling, S.W. and Nix, D.A. (2001), "Vibration-based structural damage identification", *Philos. T. R. Soc. A.*, **359**(1778), 131-149.
- Fister, I., Yang, X.S. and Brest, J. (2013), "A comprehensive review of firefly algorithms", *Swarm Evol. Comput.*, **13**, 34-46.
- Fugate, M.L., Sohn, H. and Farrar, C.R. (2001), "Vibration-based damage detection using statistical process control", *Mech. Syst. Signal Pr.*, **15**(4), 707-721.
- Gul, M. and Catbas, F.N. (2011), "Structural health monitoring and damage assessment using a novel time series analysis methodology with sensor clustering", *J. Sound Vib.*, **330**(6), 1196-1210.
- Jung, S., Ok, S.Y. and Song, J. (2010), "Robust structural damage identification based on multi - objective optimization", *Int. J. Numer. Meth. Eng.*, **81**(6), 786-804.
- Li, A.Q., Ding, Y.L., Wang, H. and Guo, T. (2012), "Analysis and assessment of bridge health monitoring mass data-progress in research/development of structural health monitoring", *Sci. China Technol. Sc.*, **55**(8), 2212-2224.
- Li, H., Ou, J.P., Zhang, X.G., Pei, M.S. and Li, N. (2015), "Research and practice of health monitoring for long-span bridges in the mainland of China", *Smart Struct. Syst.*, **15**(3), 555-576.
- Li, H.N., Yi, T.H., Gu, M. and Huo, L.S. (2009), "Evaluation of earthquake-induced structural damages by wavelet transform", *Prog. Nat. Sci-Mater.*, **19**(4), 461-470.
- Marler, R.T. and Arora, J.S. (2004), "Survey of multi-objective optimization methods for engineering", *Struct. Multidiscip. O.*, **26**(6), 369-395.
- Ou, J.P. and Li, H. (2010), "Structural health monitoring in mainland China: review and future trends", *Struct. Health Monit.*, **9**(3), 219-231.
- Shirazi, M.N., Mollamahmoudi, H. and Seyedpoor, S.M. (2014), "Structural damage identification using an adaptive multi-stage optimization method based on a modified particle swarm algorithm", *J. Optimiz. Theory Appl.*, **160**(3), 1009-1019.
- Tang, H., Zhang, W., Xie, L. and Xue, S. (2013), "Multi-stage approach for structural damage identification using particle swarm optimization", *Smart Struct. Syst.*, **11**(1), 69-86.
- Wang, H., Li, A.Q. and Li, J. (2010), "Progressive finite element model calibration of a long-span suspension bridge based on ambient vibration and static measurements", *Eng. Struct.*, **32**, 2546-2556.
- Wang, H., Li, A.Q., Guo, T. and Tao, T.Y. (2014), "Establishment and application of the wind and structural health monitoring system for the Runyang Yangtze River Bridge", *J. Shock Vib.*, **2014**, 1-15.
- Yan, Y.J., Cheng, L., Wu, Z.Y. and Yam, L.H. (2007), "Development in vibration-based structural damage detection technique", *Mech. Syst. Signal Pr.*, **21**(5), 2198-2211.
- Yang, X.S. (2010), "Firefly algorithm, stochastic test functions and design optimization", *Int. J. Bio-Inspired Comput.*, **2**(2), 78-84.
- Yang, X.S. (2014), "Swarm intelligence based algorithms: a critical analysis", *Evol. Intelligence*, **7**(1), 17-28.
- Yang, X.S., Deb, S., Hanne, T. and He, X. (2015), "Attraction and diffusion in nature-inspired optimization algorithms", *Neural Comput. Appl.*, 1-8.
- Ye, X.W., Ni, Y.Q., Wai, T.T., Wong, K.Y., Zhang, X.M. and Xu, F. (2013), "A vision-based system for dynamic displacement measurement of long-span bridges: algorithm and verification", *Smart Struct. Syst.*, **12**(3-4), 363-379.
- Ye, X.W., Ni, Y.Q., Wong, K.Y. and Ko, J.M. (2012), "Statistical analysis of stress spectra for fatigue life assessment of steel bridges with structural health monitoring data", *Eng. Struct.*, **45**, 166-176.
- Yi, T.H., Li, H.N. and Gu, M. (2011), "Optimal sensor placement for structural health monitoring based on multiple optimization strategies", *Struct. Des. Tall Spec.*, **20**(7), 881-900.
- Yi, T.H., Li, H.N. and Sun, H.M. (2013), "Multi-stage structural damage diagnosis method based on 'energy-damage' theory", *Smart Struct. Syst.*, **12**(3-4), 345-361.

- Yi, T.H., Li, H.N. and Wang, C.W. (2016), "Multiaxial sensor placement optimization in structural health monitoring using distributed wolf algorithm", *Struct. Control Health Monit.*, **23**(4), 719-734.
- Yi, T.H., Li, H.N. and Zhang, X.D. (2012), "Sensor placement on Canton Tower for health monitoring using asynchronous-climb monkey algorithm", *Smart Mater. Struct.*, **21**(12), 125023.
- Yu, L and Xu, P. (2011), "Structural health monitoring based on continuous ACO method", *Microelectron. Reliab.*, **51**(2), 270-278.
- Yu, L. and Li, C. (2014), "A global artificial fish swarm algorithm for structural damage detection", *Adv. Struct. Eng.*, **17**(3), 331-346.
- Yu, L. and Lin, J.C. (2015), "Cloud computing-based time series analysis for structural damage detection", *J. Eng. Mech. - ASCE*, 10.1061/(ASCE)EM.1943-7889.0000982 , C4015002.
- Yu, L. and Yin, T. (2010), "Damage identification in frame structures based on FE model updating", *J. Vib. Acoust. Trans ASME*, **132**(5), 051007.
- Yu, L. and Zhu, J.H. (2015), "Nonlinear damage detection using higher statistical moments of structural responses", *Struct. Eng. Mech.*, **54**(2), 221-237.
- Yu, L. and Zhu, J.H. (2016), "Structural damage prognosis on truss bridges with end connector bolts", *J. Eng. Mech. - ASCE*, 10.1061/(ASCE)EM.1943-7889.0001052 , B4016002.
- Yu, L., Xu, P. and Chen, X. (2012), "A SI-based algorithm for structural damage detection", *Proceedings of the Advances in Swarm Intelligence - Third International Conference*, Shenzhen, China. 17-20, June, 2012. (Eds., Y. Tan, Y. Shi, and Z. Ji): ICSI 2012, Part I, LNCS 7331, pp. 21-28.